This article has been accepted for publication in a future issue of this journal, but has not been fully edited. Content may change prior to final publication. Citation information: DOI 10.1109/JSEN.2019.2949367, IEEE Sensors Journal

Joint Angle and Range Estimation with Signal Clustering in FMCW Radar

Wen-Hsien Fang and Li-Der Fang
Department of Electronic and Computer Engineering
National Taiwan University of Science and Technology, Taipei, Taiwan, R.O.C.
Email: {whf, d10002206}@mail.ntust.edu.tw

***Abstract*—In this paper, we consider a simple, yet accurate approach for angle and range estimation of multiple targets in the frequency-modulated continuous-wave (FMCW) radar systems. Our new algorithm starts with estimation of time delays and ranges by the estimation of signal parameter via rotational invariance techniques (ESPRIT) algorithm. According to the estimated time delays, a group of filters is then devised to divide the received signals into a number of clusters. Finally, ESPRIT is invoked again to estimate the angles of the targets in each cluster. The new algorithm possesses some advantageous features. First, the number of the receive antennas could be less than that of the targets. Second, it is still applicable even when some targets are located at the same ranges or angles. Third, the estimated ranges and angles are automatically paired together. Both numerical simulations and practical experiments are conducted to demonstrate the superiority of our algorithm over the state-of-the-art works in terms of accuracy in various scenarios.**

***Index Terms*—range estimation, angle estimation, ESPRIT, signal clustering, range-angle estimation, FMCW radar.**

I. Introduction

Miscellaneous frequency-modulated continuous-wave (FMCW) radar based devices such as lane change assistance and cruise control have been widely used in vehicle safety systems [1]–[3]. To provide adequate information of the adjacent cars to the drivers, a central issue is to obtain the ranges and angles of the targets from the signals received by the antenna array implanted on the cars. Therefore, it is of great importance to precisely estimate these two parameters in the nowadays popular FMCW radar systems.

A variety of algorithms has been addressed to estimate the ranges and the angles, either individually or jointly, from the received signals. For range estimation, the discrete Fourier transform (DFT) is the most straightforward approach due to its simplicity and efficient implementation [4]–[6]. However, its performance is limited by the length of the data record. Another popular approach is the subspace based algorithms [7]–[10]. For example, Belfiori *et al.* [11] proposed a two-dimensional (2-D) multiple signal classification (MUSIC) for range and angle estimation. It, however, calls for heavy computations due to the computationally expensive search process. To lower the complexity, Kim *et al.* [12] addressed a DFT-ESPRIT algorithm, which first estimated the range of the targets by the one-dimensional (1-D) DFT and then the angles by ESPRIT. Its performance, however, is in general not quite satisfactory. Additionally, the number of targets needs to be less than that of the receive antennas, imposed by the standard subspace algorithms. This is a strict limitation, as it is unlikely to install lots of antennas in the vehicle FMCW radar systems due to the cost and space limitation. To resolve this setback, Oh *et al.* [13] considered a lower complexity, auto-paired 2-D estimation of signal parameter via rotational invariance techniques (ESPRIT) algorithm for joint estimation of these two parameters. Although [13] is free of the 2-D search, a computationally demanding higher-dimensional eigenvalue decomposition (EVD) is still required, so the complexity is still not light. A similar dual smoothing algorithm was addressed in [14], which constructed two dual smoothed matrices and then utilized the shift invariance structure to estimate the angles and delays, respectively. Despite that it can attain more accurate parameter estimates than [12] and [13], the size of the dual smoothed Hankel matrix is not small, entailing lots of computations in EVD. Also, [12]- [14] are not applicable when some of the targets are at the same ranges.

To achieve satisfactory performance with modest complexity, in this paper we consider a simple, yet accurate approach for range and angle estimation of multiple targets in the FMCW radar systems. The new algorithm starts with the estimation of time delays and ranges of the targets by establishing a Hankel matrix based on the received signals. ESPRIT is then employed for time delay and range estimation. Afterward, according to the estimated time delays, we develop a group of filters to divide the received signals into different clusters. Finally, ESPRIT is invoked again to estimate the angles of the targets. With such a signal clustering process, the estimation accuracy is boosted due to less interfering signals. The complexity is reduced as well because now EVD is with respect to smaller matrices. Additionally, the new algorithm possesses some advantageous features. First, the number of the receive antennas could be less than that of the targets, as the number of targets is less in each cluster after the clustering process. Second, it is still applicable even when some targets are located at the same ranges or angles. Third, the estimated ranges and angles are automatically paired together without extra efforts. Both of the numerical simulations and practical experiments are conducted to demonstrate the superiority of our algorithm over the state-of-the-art works in terms of accuracy in various scenarios.

This paper is structured as follows. Sec. II introduces the system model of the FMCW radar. Sec. III depicts our new algorithm for combined range and angle estimation. Numerical

1558-1748 (c) 2019 IEEE. Personal use is permitted, but republication/redistribution requires IEEE permission. See http://www.ieee.org/publications_standards/publications/rights/index.html for more information.

This article has been accepted for publication in a future issue of this journal, but has not been fully edited. Content may change prior to final publication. Citation information: DOI 10.1109/JSEN.2019.2949367, IEEE Sensors Journal

simulations and practical experiments are provided respectively in Secs. IV and V to verify the proposed algorithm. Sec. VI draws some remarks to conclude the paper.

II. SYSTEM MODEL

Consider an FMCW radar system, which has one transmit antenna and Q uniformly spaced receive antennas by a range of d. The block diagram of the receive chain of this system is as shown in Fig. 1. Assume that there are M narrowband targets, the signal received by the qth antenna is then [11]

$$y_q(t) = \sum_{m=1}^{M} \alpha_m s(t-\tau_m) e^{j\frac{2\pi}{\lambda}d(q-1)\sin\theta_m} + w_q(t) \quad (1)$$

for $q = 1, ..., Q$, where τ_m, θ_m, and α_m denote respectively the time delay, the impinging angle, and the complex amplitude of the mth target, λ is the wavelength of the carrier, and $w_q(t)$ is zero-mean white Gaussian noise. The transmitted signal $s(t)$ is [14]

$$s(t) = \begin{cases} e^{j(2\pi f_c t + \pi\eta t^2)} & 0 \le t < T \\ 0 & \text{elsewise} \end{cases} \quad (2)$$

where f_c is the carrier frequency of the FMCW waveform and $\eta = B_w/T$ is the increase rate of the sawtooth shaped waveform, in which T and B_w are the period and bandwidth of the FMCW chirp waveform, respectively. The received FMCW waveforms are transformed to the sinusoidal beat signals by a de-chirping process. The beat signal at the qth receive antenna is given by

$$\begin{aligned} x_q(t) &= y_q^*(t)s(t) \\ &= \sum_{m=1}^{M} \alpha_m e^{j(2\pi\eta\tau_m t - \pi\eta\tau_m^2)} e^{j(\frac{2\pi}{\lambda}d(q-1)\sin\theta_m)} + n_q(t) \end{aligned}$$

where the superscript * denotes complex conjugation and $n_q(t)$ is the transformed white Gaussian noise. After sampling the beat signal at a rate of $f_s = 1/T_s$, the discrete-time model of $x_q(t)$ can be expressed as

$$x_q[n] = \sum_{m=1}^{M} \alpha_m \kappa_m e^{j(q-1)a_m} e^{jb_m n} + n_q[n] \quad (3)$$

for $n = 1, \ldots, N$, where $\kappa_m = e^{-j\pi\eta\tau_m^2}$, $a_m = \frac{2\pi}{\lambda} d sin\theta_m$, $b_m = \frac{2\pi\eta\tau_m}{f_s}$, N denotes the number of samples from the analog-to-digital converter (ADC), and $n_q[n]$ is the additive discrete-time white noise with variance σ^2.

III. PROPOSED ALGORITHM

This section describes a new algorithm which simultaneously estimates the ranges and angles of multiple targets in the FMCW radar systems. This algorithm, as show in Fig. 2, starts with time delay and range estimation by ESPRIT. Afterward, with the estimated time delays, a set of filters is established to separate the received signals into different clusters. Finally, ESPRIT is utilized again for each cluster to estimate the angles of the targets.

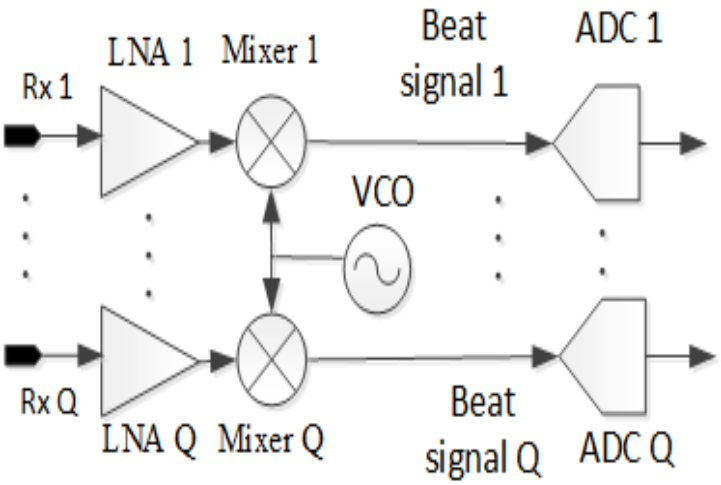

Fig. 1: Block diagram of the receive chain of a 24 GHz FMCW radar system.

A. Range Estimation

First, based on the output of the qth antenna, we construct a Hankel matrix [15] given by

$$\mathbf{X}_q = \begin{bmatrix} x_q[1] & x_q[2] & \cdots & x_q[N-L+1] \\ x_q[2] & x_q[3] & \cdots & x_q[N-L+2] \\ \vdots & \vdots & \ddots & \vdots \\ x_q[L] & x_q[L+1] & \cdots & x_q[N] \end{bmatrix} \quad (4)$$

for $q = 1, \cdots, Q$, where L is a properly chosen parameter and according to our experience we can choose $L = \frac{N}{5}$. Note that the Hankel matrix $\mathbf{X}_q$ in (4) can be factorized as

$$\mathbf{X}_q = \mathbf{B}_q \mathbf{D}_q \mathbf{C}_q^T + \mathbf{N}_q \quad (5)$$

where the superscript ^{T} denotes matrix transposition, $\mathbf{B}_q = [\alpha_1 \mathbf{b}_1, ..., \alpha_M \mathbf{b}_M]$, $\mathbf{C}_q = [\mathbf{c}_1, ..., \mathbf{c}_M]$, in which $\mathbf{b}_m = [1, e^{jb_m}, ..., e^{j(L-1)b_m}]^T$ and $\mathbf{c}_m = [1, e^{jb_m}, ..., e^{j(N-L)b_m}]^T$, $\mathbf{D}_q = \text{diag}\{\kappa_1 e^{j(q-1)a_1}, \kappa_2 e^{j(q-1)a_2}, ..., \kappa_M e^{j(q-1)a_M}\}$, and $\mathbf{N}_q$ is constructed by $n_q[n]$ in the same way as $x_q[n]$ in (4). Here we consider the covariance matrix of the received signals, as it allows us to use the white noise property, for which the noise covariance matrix is a deterministic diagonal matrix. Some sophisticated signal processing algorithms such as the subspace methods can then be utilized to render more accurate parameter estimates.

By using (5), the covariance matrix of $\mathbf{X}_q$, $\mathbf{P}_q^x := E[\mathbf{X}_q \mathbf{X}_q^H]$, is given by

$$\mathbf{P}_q^x = \mathbf{B}_q \mathbf{\Lambda}_q \mathbf{B}_q^H + (N-L+1)\sigma^2 \mathbf{I}_L \quad (6)$$

where $\mathbf{\Lambda}_q$=$E[\mathbf{D}_q \mathbf{D}_q^H]$ with the superscript ^{H} being the Hermitian operation, and we have used the facts that $\mathbf{C}^T\mathbf{C}^* = (N-L+1)\mathbf{I}_M$ and $E[\mathbf{N}_q \mathbf{N}_q^H]$=$(N-L+1)\sigma^2 \mathbf{I}_L$, in which $\mathbf{I}_L$ denotes an $L \times L$ matrix. We can then employ ESPRIT with respect to $\mathbf{P}_q^x$ to estimate the time delays. Utilizing the shift invariant property, we have

$$\mathbf{E}_{q,1} \mathbf{\Psi}_q = \mathbf{E}_{q,2} \quad (7)$$

1558-1748 (c) 2019 IEEE. Personal use is permitted, but republication/redistribution requires IEEE permission. See http://www.ieee.org/publications_standards/publications/rights/index.html for more information.

This article has been accepted for publication in a future issue of this journal, but has not been fully edited. Content may change prior to final publication. Citation information: DOI 10.1109/JSEN.2019.2949367, IEEE Sensors Journal

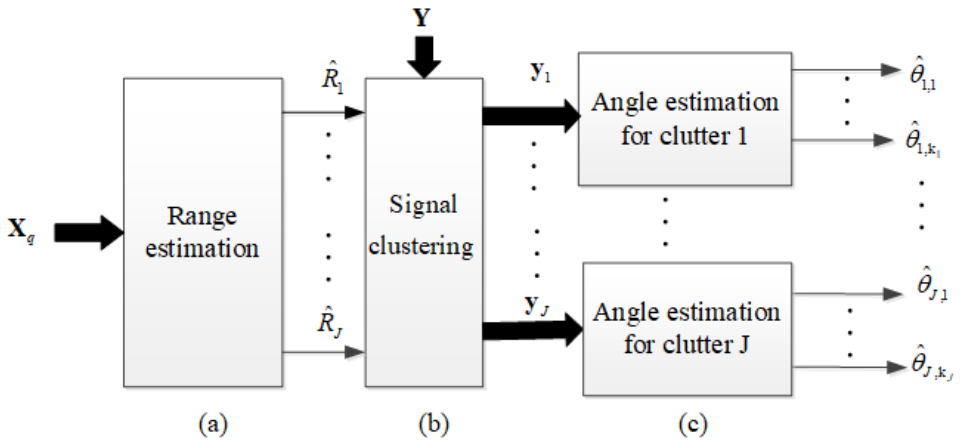

Fig. 2: Block diagram of the proposed algorithm, which consists of three steps: (a) range estimation, (b) signal clustering, and (c) angle estimation.

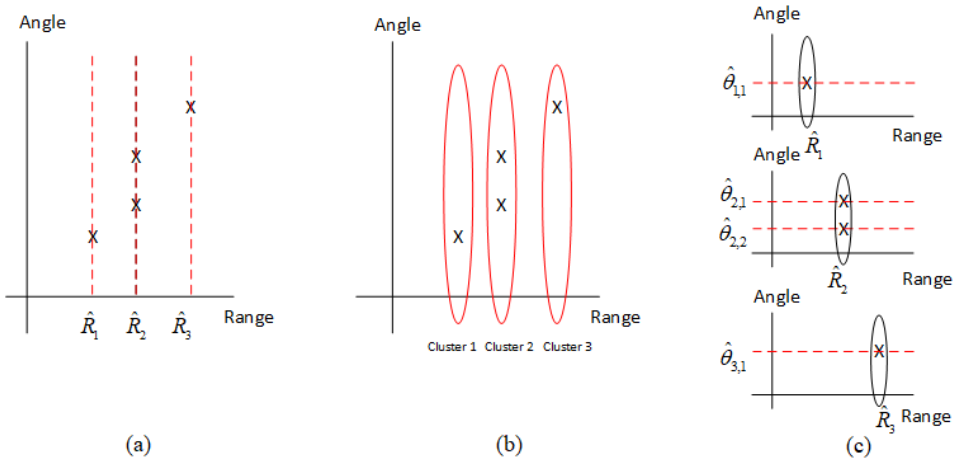

Fig. 3: A simple scenario to illustrate the three steps of the proposed algorithm, where M=4 and J=3.

where $\mathbf{\Psi}_q = \text{diag}\{e^{jb_1}, \ldots, e^{jb_M}\}$, $\mathbf{E}_{q,1} = \mathbf{J}_1\mathbf{E}_q$, and $\mathbf{E}_{q,2} = \mathbf{J}_2\mathbf{E}_q$, in which $\mathbf{J}_1$=[$\mathbf{I}_{L-1}$$\vdots$$\mathbf{0}$], $\mathbf{J}_2$=[$\mathbf{0}$$\vdots$$\mathbf{I}_{L-1}$] with $\mathbf{0}$ being a zero vector of length $(L-1)$, and $\mathbf{E}_q$ is the signal subspace which contains the eigenvectors associated with the J largest eigenvalues of $\mathbf{P}_q^x$. Also, $J \leq M$ is the number of the estimated delays. In case that all targets have distinct delays, then $J = M$. Using the least square (LS) ESPRIT, we can obtain

$$\hat{\mathbf{\Psi}}_q = \mathbf{E}_{q,1}^{\dagger}\mathbf{E}_{q,2} \tag{8}$$

where † denotes the pseudo inverse. The time delay estimates can be determined by

$$\hat{\tau}_{q,m} = \frac{f_s T}{2\pi B w} angle((\hat{\mathbf{\Psi}}_q)_{mm}), \quad m = 1, \ldots, J \tag{9}$$

where $angle(\cdot)$ denotes the angle of the (m,m)th element of $\hat{\mathbf{\Psi}}_q$.

We can take the delay estimate from any antenna, say the first one, and for notational brevity, denote $\hat{\tau}_{1,m}$ by $\hat{\tau}_m$. The range estimate of the mth target is then

$$\hat{R}_m = \frac{c\hat{\tau}_m}{2}, \quad m = 1, \ldots, J \tag{10}$$

B. Signal Clustering

Next, we divide the received signals $\{x_q[n]\}$ into J clusters with the signals in each cluster corresponding to different time delays. With such a clustering process, the estimation accuracy can be boosted, as the interfering signals are less in each cluster. Also, since only angles need to be estimated for the signals in each cluster, the computations required are alleviated. Toward this end, we collect the received signals from all of the antennas and establish a data matrix $\mathbf{Y}$ given by

$$\mathbf{Y} = \begin{bmatrix} x_1[1] & x_1[2] & \cdots & x_1[N] \\ x_2[1] & x_2[2] & \cdots & x_2[N] \\ \vdots & \vdots & \ddots & \vdots \\ x_Q[1] & x_Q[2] & \cdots & x_Q[N] \end{bmatrix} \tag{11}$$

Based on (3), $\mathbf{Y}$ can be factorized as

$$\mathbf{Y} = \sum_{i=1}^{J} \alpha_i \kappa_i \mathbf{a}(\theta_i)\boldsymbol{v}^H(\tau_i) + \bar{\mathbf{N}} \tag{12}$$

where $\mathbf{a}(\theta_i) = [1, e^{ja_i}, ..., e^{j(Q-1)a_i}]^T$, $\boldsymbol{v}(\tau_i) = [1, e^{-jb_i}, ..., e^{-j(N-1)b_i}]^T$, and $\bar{\mathbf{N}}$ is constructed by $n_q[n]$ in the same way as $x_q[n]$ in (11).

1558-1748 (c) 2019 IEEE. Personal use is permitted, but republication/redistribution requires IEEE permission. See http://www.ieee.org/publications_standards/publications/rights/index.html for more information.

This article has been accepted for publication in a future issue of this journal, but has not been fully edited. Content may change prior to final publication. Citation information: DOI 10.1109/JSEN.2019.2949367, IEEE Sensors Journal

Using the estimated time delays $\{\hat{\tau}_1, ..., \hat{\tau}_J\}$, we can construct a group of filters $\mathbf{w}_j,\ j = 1, ..., J$, to divide the received signals into J clusters. For this, we minimize the noise power after passing through the filter $\mathbf{w}_j$ while keeping the target with delay $\hat{\tau}_j$ intact and annihilating the targets with delays $\hat{\tau}_1, ..., \hat{\tau}_{j-1}, \hat{\tau}_{j+1}, \ldots, \hat{\tau}_J$, *i.e.*, $\boldsymbol{v}^H(\hat{\tau}_i)\mathbf{w}_j = \delta_{i,j}$, where $\delta_{i,j}$ is the Kronecker delta function:

$$\delta_{i,j} = \begin{cases} 1 & i = j \\ 0 & \text{elsewhere} \end{cases}$$

Since the output of the noise power $E[\left\|\bar{\mathbf{N}}\mathbf{w}_j\right\|^2] = \mathbf{w}_j^H E[\bar{\mathbf{N}}^H\bar{\mathbf{N}}]\mathbf{w}_j = Q\|\mathbf{w}_j\|^2\sigma^2$, where $\|\cdot\|$ denotes the Euclidean norm, as the noise is assumed to be white, the determination of $\mathbf{w}_j$ can then be posted as the following constrained optimization problem:

$$\min_{\mathbf{w}_j}\ \mathbf{w}_j^H\mathbf{w}_j \quad \text{under} \quad \mathbf{G}^H\mathbf{w}_j = \mathbf{e}_j, \quad j = 1, ..., J \tag{13}$$

where $\mathbf{G} = [\mathbf{b}(\hat{\tau}_1), ..., \mathbf{b}(\hat{\tau}_J)]$ and $\boldsymbol{e}_j$ is a $J\times 1$ vector with the jth entry being equal to one and zeros elsewhere. The solution of $\mathbf{w}_j$ can be readily shown to be [16]–[18]

$$\mathbf{w}_j = \boldsymbol{G}(\boldsymbol{G}^H\boldsymbol{G})^{-1}\mathbf{e}_j, \quad j = 1, 2, ..., J \tag{14}$$

Postmultiplying $\mathbf{Y}$ by $\mathbf{w}_j$, we can then decompose the received signals into J clusters given by

$$\mathbf{y}_j = \mathbf{Y}\mathbf{w}_j \approx \sum_{k=1}^{K_j}\alpha_k\kappa_k\mathbf{a}(\theta_k) + \bar{\mathbf{n}}_j, \quad j = 1, ..., J \tag{15}$$

where K_j denotes the number of targets in the jth cluster, $\bar{\mathbf{n}}_j = \bar{\mathbf{N}}\mathbf{w}_j$, and we have used the fact that $\boldsymbol{v}^H(\tau_i)\mathbf{w}_j \approx 0$, $i \neq j,\ i = 1, \ldots, M,\ i = 1, \ldots, J$.

C. Angle Estimation

Finally, we estimate the angles of the targets in each cluster. To achieve this, we reconstruct a Hankel matrix for each cluster $\mathbf{y}_j$ by

$$\mathbf{Z}_j = \begin{bmatrix} y_j[1] & y_j[2] & \cdots & y_j[Q-LL+1] \\ y_j[2] & y_j[3] & \cdots & y_j[Q-LL+2] \\ \vdots & \vdots & \ddots & \vdots \\ y_j[LL] & y_j[LL+1] & \cdots & y_j[Q] \end{bmatrix} \tag{16}$$

where LL is a properly chosen parameter and according to our experience we can choose $LL = Q/2+1$. Based on (16), the covariance matrix of the signal in the jth cluster, $\mathbf{P}_j^z := \frac{1}{N}E[\mathbf{Z}_j\mathbf{Z}_j^H]$, can be expressed as

$$\mathbf{P}_j^z = \sum_{k=1}^{K_j}|\alpha_k\kappa_k|^2\mathbf{a}(\theta_k)\mathbf{a}^H(\theta_k) + \bar{\sigma}^2\mathbf{I}_{LL}, \quad j = 1, \ldots J \tag{17}$$

where the noise covariance matrix $E[\bar{\mathbf{n}}_j\bar{\mathbf{n}}_j^H] = \bar{\sigma}^2\mathbf{I}_{LL}$, in which $\bar{\sigma}^2 = Q||\mathbf{w}_j||^2\sigma^2$. This fact can be proved by considering the (k,l)th component of $E[\bar{\mathbf{n}}_j\bar{\mathbf{n}}_j^H]$:

$$\begin{aligned} &\sum_{i=1}^{N}\sum_{n=1}^{N}\bar{\mathbf{N}}(k,i)\mathbf{w}_j(i)\bar{\mathbf{N}}^*(l,n)\mathbf{w}_j^*(n) \\ &= \sum_{i=1}^{N}\bar{\mathbf{N}}(k,i)\mathbf{w}_j(i)\bar{\mathbf{N}}^*(l,i)\mathbf{w}_j^*(i) \\ &= Q||\mathbf{w}_j||^2\sigma^2\delta_{k,l} \end{aligned}$$

where the simplification is due to the fact that $\bar{\mathbf{N}}$ is white noise. Along the same line as above, invoking LS ESPRIT again for each cluster, we can obtain the angle estimates, say $\hat{\theta}_{j,l},\ j = 1, \ldots, J,\ l = 1, \ldots, K_j$.

To illustrate the developed algorithm, we consider a simple scenario, where there are $M = 4$ targets with the constellation of (range, angle) as shown in Fig. 3, where two of them are located at the same range. Using our algorithm, we can obtain $J = 3$ delay and range estimates, $\hat{R}_1$, $\hat{R}_2$, and $\hat{R}_3$, as shown in Fig. 3 (a) after range estimation in Step 1. With these three delay estimates, we can establish three filters, each of which corresponds to a delay estimate. Utilizing these three filters, we can decompose the received signals into 3 clusters, as shown in Fig. 3 (b), where the first cluster (corresponds to $\hat{R}_1$) has only one target signal, the second cluster (corresponds to $\hat{R}_2$) has two target signals as these two targets are located at the same range, and the third cluster (corresponds to $\hat{R}_3$) also has one target signal. Finally, ESPRIT is carried out again, but with respect to each of these three clusters. We can then obtain angle estimates: $\theta_{1,1}$ for the target in the first cluster ($K_1 = 1$), $\theta_{2,1}$ and $\theta_{2,2}$ for the ones in the second cluster ($K_2 = 2$), and $\theta_{3,1}$ for the one in the third cluster ($K_3 = 1$). The resulting parameter estimates $\{(\hat{R}_1, \hat{\theta}_{1,1}), (\hat{R}_2, \hat{\theta}_{2,1}), (\hat{R}_2, \hat{\theta}_{2,2}), (\hat{R}_3, \hat{\theta}_{3,1})\}$ are automatically associated with the four targets. For reference, the overall procedures of the proposed algorithm are summarized in Fig. 4.

The proposed algorithm involves two parameters, L and LL, which determine the size of the constructed Hankel matrices in (4) and (16), respectively, and leverages the complexity and performance. First, we can note that L in (4) is related to the estimation of the *temporal* parameter, time delay, and depends only on the number of samples from the ADC, N. Since N is in general fairly large (say a few hundred), we can thus choose a small fraction of N, say $L = N/5$, in the simulations. This is because there are now enough numbers of rows (sliding data segments) in the Hankel matrix to achieve satisfactory performance and meanwhile the computational complexity can still be kept low. On the other hand, LL in (16) is related to the estimation of the *spatial* parameter, impinging angle, and depends only on the number of the receive antenna, Q. Since Q is in general small due to the cost and the space limitation, we need to choose around one half of Q, say $LL = Q/2+1$, to make full use of the available data to achieve satisfactory performance.

D. Comparison with the State-of-the-Art Methods

In this section, we compare the new algorithm, referred to as clustered ESPRIT, and three state-of-the-art works, DFT-ESPRIT [12], 2D-ESPRIT [13], and the dual smoothing algorithm [14], from various aspects.

First, we consider the pairing issue of the estimated ranges and angles, as all of these four algorithms estimate distance and delay separately. The pairing of these two parameters is automatically achieved by 2D-ESPRIT, as it conducts EVDs with respect to the same covariance matrix. For the proposed clustered ESPRIT, the estimated ranges and angles are also

1558-1748 (c) 2019 IEEE. Personal use is permitted, but republication/redistribution requires IEEE permission. See http://www.ieee.org/publications_standards/publications/rights/index.html for more information.

This article has been accepted for publication in a future issue of this journal, but has not been fully edited. Content may change prior to final publication. Citation information: DOI 10.1109/JSEN.2019.2949367, IEEE Sensors Journal

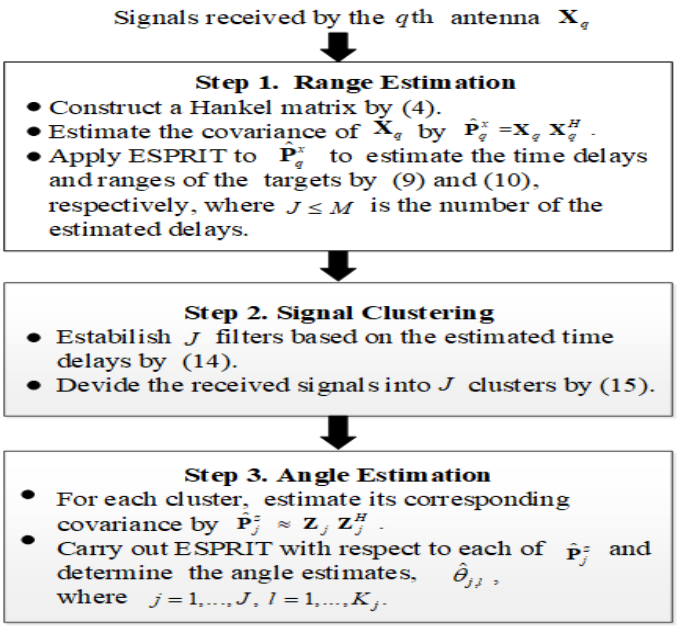

Fig. 4: Summary of the proposed algorithm.

automatically paired together due to the clustering process, as shown in Fig. 3. However, for DFT-ESPRIT and the dual smoothing algorithm, these two parameters need to be properly paired together by extra manipulations.

For the restriction on the locations of the targets, the proposed algorithm is still applicable even when some targets are located at the same ranges. This is because it includes a clustering process in between the range and the angle estimation. In contrast, all of the other three baselines are not applicable in this scenario due to the rank deficiency problem.

Next, we scrutinize the complexity of these algorithms in terms of the number of multiplications [19] and the CPU time required, where for fairness we assume that the ranges of all targets are different. First, DFT-ESPRIT requires $NlogN$ and $Q^2M + \frac{1}{3}Q^3$ multiplications for the estimation of ranges and angles, respectively. Since in general $N >> M, Q$, so DFT-ESPRIT requires approximately $NlogN$ multiplications. 2D-ESPRIT roughly requires $\frac{2Q^2N^3}{27}$ multiplications. For the dual smoothing algorithm, it requires to perform EVD twice to estimate the ranges and angles, which respectively call for $Q^2L_c^2L_r + QL_cL_r^2 + L_r^3 + \frac{1}{3}M^3$ and $4Q^2(L_c-1)^2L_r + 2Q(L_c-1)Lr^2 + L_r^3 + \frac{1}{3}M^3$ multiplications. It is suggested in [14] to choose the parameter $L_c = \frac{1}{2}L_r = N/3$ to achieve better performance, so it roughly requires $\frac{10Q^2N^3}{27}$ multiplications. As for the proposed clustered ESPRIT, it requires $L^2(N-L)+\frac{1}{3}L^3$ multiplications for range estimation, $NM^2 + NM$ multiplications for the construction of the clustering filters, MQN multiplications for signal clustering, and $MQ^2 + \frac{1}{3}Q^3$ multiplications for conducting ESPRIT for angle estimation. If we use the optimal L, *i.e.* $L = \frac{N}{5}$, then it requires roughly $\frac{N^3}{28}$ multiplications. Consequently, DFT-ESPRIT calls for the lowest complexity, as it estimates the delays by DFT, which can be readily computed by the fast Fourier transform. Both of 2D-ESPRIT and the dual smoothing algorithm require much higher complexity than DFT-ESPRIT and the proposed algorithm. This is because both algorithms stack the data into similar large dual smoothed matrices to achieve satisfactory estimation accuracy and overcome the antenna limitation imposed by the subspace algorithms, leading to heavy computational load. While the computational overhead of the new algorithm is higher than DFT-ESPRIT, it is substantially lower than 2D-ESPRIT and the dual smoothing algorithm, as EVD is with respect to much smaller matrices.

To further justify the complexity, we also compare the CPU time with different numbers of antennas, Q, when $N = 250$, as shown in Fig. 5, from which we can see that it is consistent with the numbers of multiplications derived above. The comparison of the CPU time with different numbers of samples, N, when $Q = 2$, is furnished as well in Fig. 6. Again, we can also see that it is in line with the above expressions.

For easy reference, comparisons of the proposed algorithm and the three baselines are summarized in Table 1.

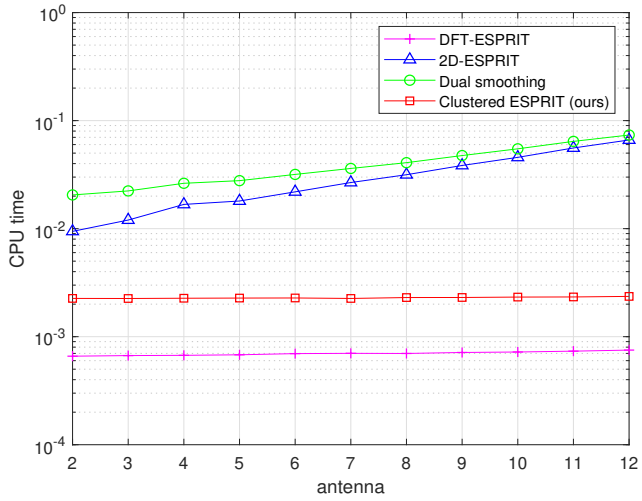

Fig. 5: CPU time versus different numbers of antennas Q.

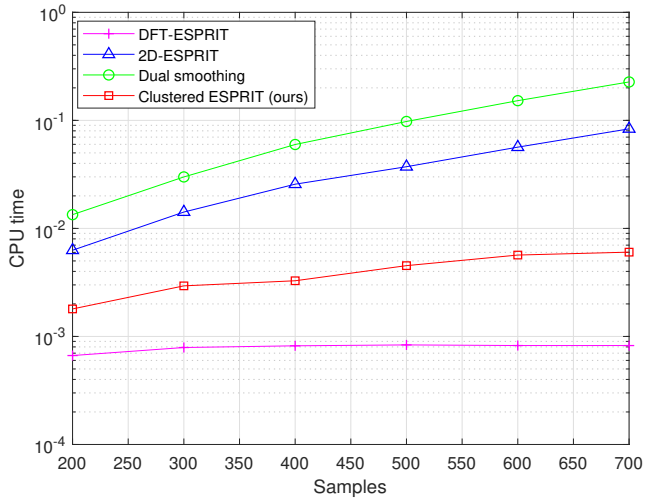

Fig. 6: CPU time versus different numbers of samples N.

1558-1748 (c) 2019 IEEE. Personal use is permitted, but republication/redistribution requires IEEE permission. See http://www.ieee.org/publications_standards/publications/rights/index.html for more information.

This article has been accepted for publication in a future issue of this journal, but has not been fully edited. Content may change prior to final publication. Citation information: DOI 10.1109/JSEN.2019.2949367, IEEE Sensors Journal

TABLE I: Comparisons of the proposed algorithm with the state-of-the-art methods, where N and Q denote the number of samples and the number of antennas, respectively.

Algorithm	Multiplication no.	Automatic pairing	Targets with same ranges or angle?
DFT-ESPRIT	$Nlog(N)$	no	no
2D-ESPRIT	$\frac{2Q^2N^3}{27}$	yes	no
Dual-smoothing	$\frac{10Q^2N^3}{27}$	no	no
Ours	$\frac{N^3}{28}$	yes	yes

IV. NUMERICAL SIMULATIONS

Next, we carry out some numerical simulations to assess the proposed clustered ESPRIT in comparison with the aforementioned three baselines, 2D-ESPRIT [13], DFT-ESPRIT [12] and the dual smoothing algorithm [14]. The data model is as considered in Sec. II. For reference, the Cramer-Rao low bound (CRLB) [20] is also included, which serves as the theoretically optimum lower bound for the parameter estimation problems. The root-mean-square-error (RMSE) is used as the performance metric, defined as $\sqrt{\frac{1}{M}\sum_{m=1}^{M}\left(\tau_m-\hat{\tau}_m\right)^2}$ and $\sqrt{\frac{1}{M}\sum_{m=1}^{M}\left(\theta_m-\hat{\theta}_m\right)^2}$ for the time delay and angle estimates, respectively. For every signal-to-noise-ratio (SNR), 200 Monte Carlo simulations are conducted. The number of samples N is chosen as 250.

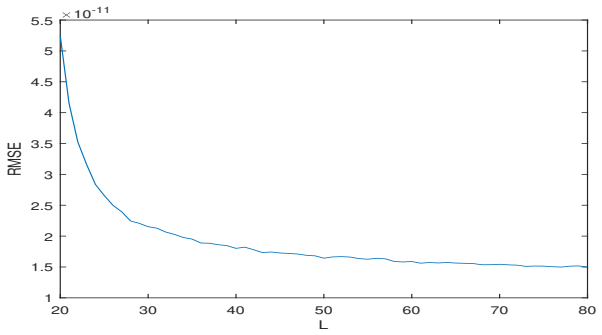

Fig. 7: RMSE of the delay estimates versus L at SNR=0 dB with $Q = 10$ in Ex. 1.

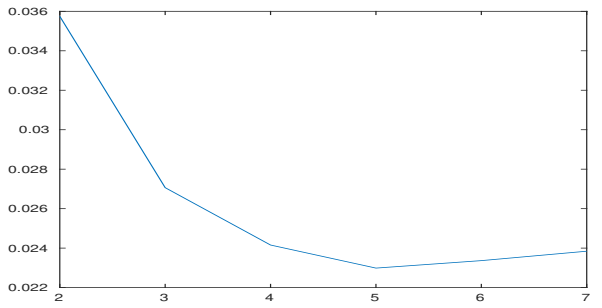

Fig. 8: RMSE of the angle estimates versus LL at SNR=0 dB with $Q = 10$ in Ex. 1.

To follow we consider two scenarios: all targets are located at different ranges or some of them are at the same ranges.

Example 1 (All targets with different ranges)

Assume that there are $M = 5$ targets which are located at $(R_1, \theta_1) = [3\,m, -50^o]$, $(R_2, \theta_2) = [7\,m, -25^o]$, $(R_3, \theta_3) = [9\,m, 15^o]$, $(R_4, \theta_4) = [12\,m, 45^o]$, and $(R_5, \theta_5) = [17\,m, 55^o]$, exactly the same scenario as considered in [14]. We conduct two cases with the number of receive antennas Q being chosen as 10 and 2.

We first assess the choice of the parameters L and LL. To this end, we compare the RMSEs of the delay estimates based on the proposed algorithm versus L with $Q = 10$ at SNR=0 dB, as shown in Fig. 7, from which we can see that the RMSEs decrease with the increase of L and reach a constant when L is around $\frac{N}{5} = 50$. To lower the complexity, we thus choose $L = \frac{N}{5}$. Based on this value of L, next we compare the RMSEs of the angle estimates versus LL, as shown in Fig. 8, from which we can see that the RMSEs attain the lowest at around $LL = \frac{Q}{2} + 1 = 6$. This again verifies our choice of this parameter. Based on these observations, in the following simulations, we will choose L and LL according to these two rules.

We begin with a comparison of the RMSEs of the time delay and angle estimates using the aforementioned algorithms, as shown in Figs. 9 and 10, respectively, with $Q = 10$, which is more than the number of targets. The parameters L and LL in the proposed algorithm are set as 50 and 6, respectively, as suggested above. We can note from Figs. 9 and 10 that the performance of the proposed algorithm and other ESPRIT-based baselines deteriorates or even exhibits an error floor when SNR $\leq$ -5 dB with the proposed algorithm suffering the least performance degradation. It is as expected because it is known that the subspace based algorithms do not work well under very low SNR scenarios. We can also see that DFT-ESPRIT in general provides the worst delay estimation, as the accuracy of the DFT-based approach is limited by the number of the available data samples. However, unlike the subspace methods, DFT approach is less sensitive to the SNRs. All of the dual smoothing algorithm, 2D-ESPRIT, and the proposed clustered ESPRIT use the high-resolution subspace algorithm, ESPRIT, so they can produce much better performance with clustered ESPRIT being a bit better. For the angle estimation, we can notice from Fig. 10 that all algorithms can successfully estimate the angles of the targets, as now there are more receive antennas than the number of targets. All DFT-ESPRIT, 2D-ESPRIT, and the dual smoothing algorithm provide close performance, since all of them employ similar signal rotational invariance properties for angle estimation. The performance of the proposed clustered ESPRIT is superior to these three baselines with the incorporation of a signal clustering process to mitigate the interfering signals in the angle estimation process.

As a more vivid illustration, we provide the range-angle map of the targets based on these algorithms at SNR=0 dB, as shown in Fig. 14, from which we can see that DFT-ESPRIT is not applicable here, so the estimates exhibit a large deviation from the true target location. Compared with 2D-ESPRIT and the dual smoothing algorithm, the estimates based on the

1558-1748 (c) 2019 IEEE. Personal use is permitted, but republication/redistribution requires IEEE permission. See http://www.ieee.org/publications_standards/publications/rights/index.html for more information.

This article has been accepted for publication in a future issue of this journal, but has not been fully edited. Content may change prior to final publication. Citation information: DOI 10.1109/JSEN.2019.2949367, IEEE Sensors Journal

proposed algorithm are well centered around the true location. These observations are in agreement with the outcomes in Figs. 12 and 13.

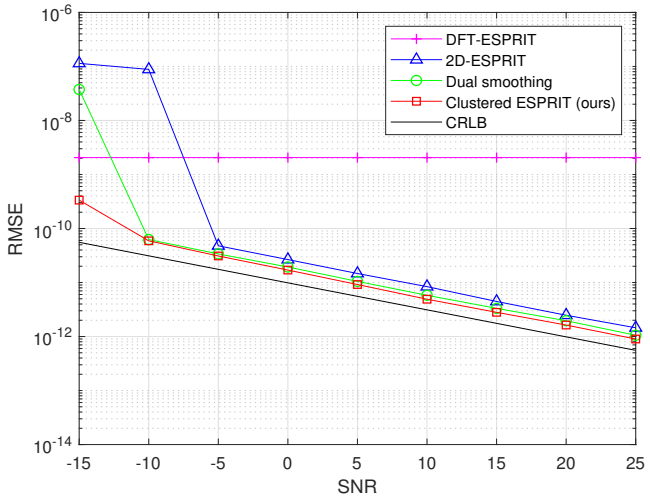

Fig. 9: RMSE of the time delay estimates versus SNR with $Q = 10$ in Ex. 1.

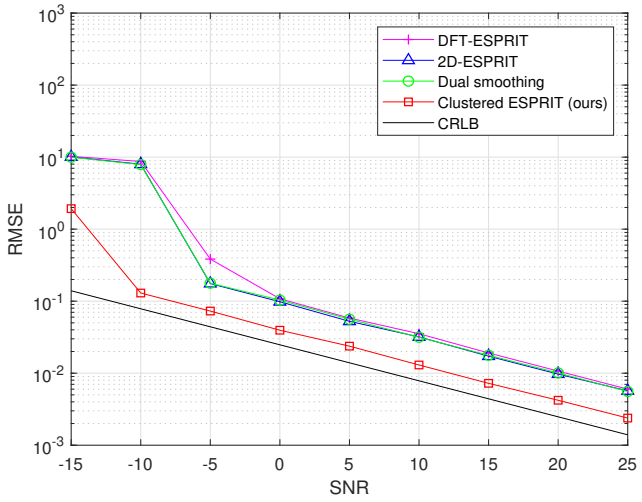

Fig. 10: RMSE of the angle estimates versus SNR with $Q = 10$ in Ex. 1.

Next, we compare the RMSEs of the time delay and angle estimates using the aforementioned algorithms, as shown in Figs. 9 and 10, respectively, but with $Q = 2$, which is now less than the number of targets. The parameters L and LL in the proposed algorithm are set as 50 and 2, respectively, as suggested above. We can see from Fig. 9 that all of these algorithms can precisely estimate the time delays, but ESPRIT-based algorithms again yield superior performance over DFT-based algorithm. For the angle estimation, we can see from Fig. 13 that DFT-ESPRIT fails in this scenario. This is because now there are $M = 5$ targets but with only two receive antennas, so it can not work in this situation. On the other hand, both 2D-ESPRIT and the dual smoothing

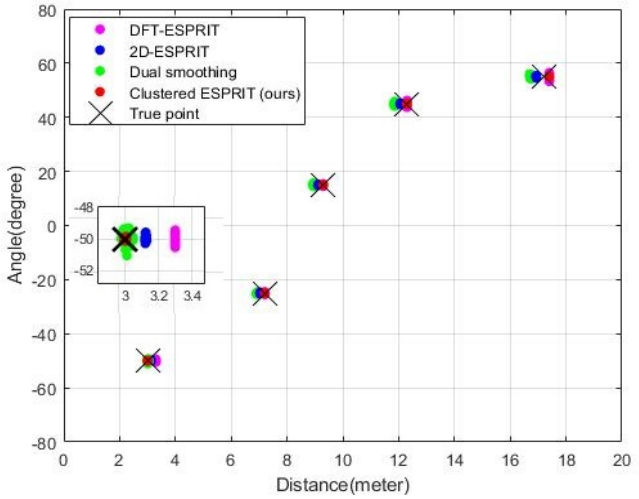

Fig. 11: The range-angle map of the targets with $Q = 10$ at SNR=0 dB in Ex. 1.

algorithm stack the data into similar dual smoothed Hankel matrices to overcome the shortage of the receive antennas in this scenario. The proposed clustered ESPRIT, which includes a signal clustering process in between the range and angle estimation, can also circumvent such a limitation and is still applicable in this scenario. We can also see that the proposed clustered ESPRIT outperforms these two algorithms, as there is only one target in each cluster and thus the angle of each target can be precisely estimated.

Again, for a more vivid illustration, we provide the range-angle map of the targets based on these algorithms at SNR=0 dB, as shown in Fig. 11, from which we can see that all algorithms can well estimate the ranges and angles of these targets. Also, the proposed clustered ESPRIT surpasses the others with the smallest deviations from the true target locations. These results are again in consistence with the observations in Figs. 9 and 10.

Example 2 (Some targets with the same ranges)

Next, we consider the scenario where some targets are at the same ranges. Assume that there are $M = 5$ targets which are located at $(R_1, \theta_1) = [3\,m, -50^o]$, $(R_2, \theta_2) = [7\,m, -25^o]$, $(R_3, \theta_3) = [7\,m, 15^o]$, $(R_4, \theta_4) = [12\,m, 45^o]$, and $(R_5, \theta_5) = [17\,m, 55^o]$, where the 2nd and the 3rd targets are located at the same range. The parameters for simulation are the same as the above two except that the number of receive antennas Q is 4 and LL=3. The comparison of the RMSEs of the time delay and angle estimates are shown in Fig. 15 and Fig. 16, respectively, and the range-angle map at SNR=0 dB is as shown in Fig. 17. We can note again from Figs. 15 and 16 that the performance of the proposed algorithm and other ESPRIT-based baselines deteriorates or even exhibits an error floor under very low SNR scenarios. Also, we can see from these figures that these three baselines are not applicable for the angle estimation. In contrast, the proposed cluster-ESPRIT can still work in this scenario.

1558-1748 (c) 2019 IEEE. Personal use is permitted, but republication/redistribution requires IEEE permission. See http://www.ieee.org/publications_standards/publications/rights/index.html for more information.

This article has been accepted for publication in a future issue of this journal, but has not been fully edited. Content may change prior to final publication. Citation information: DOI 10.1109/JSEN.2019.2949367, IEEE Sensors Journal

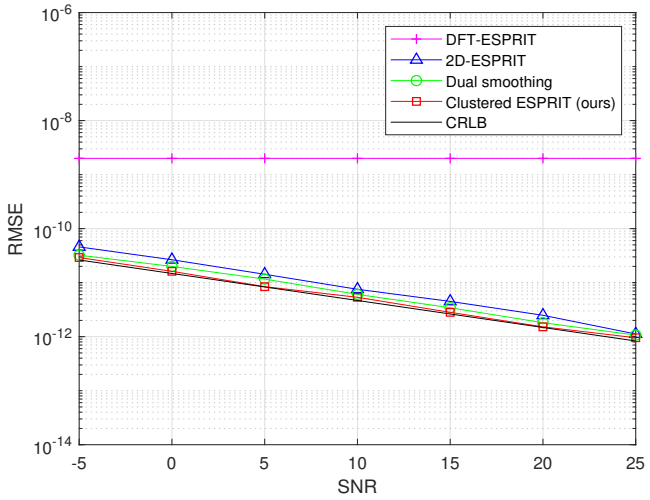

Fig. 12: RMSE of the time delay estimates versus SNR with $Q = 2$ in Ex. 1.

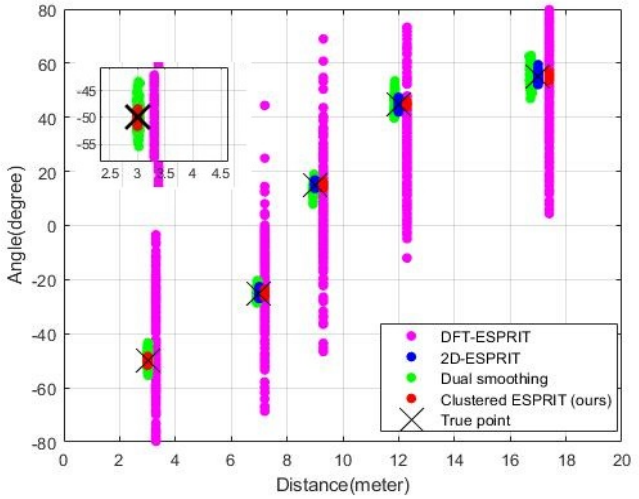

Fig. 14: The range-angle map of the targets with $Q = 2$ at SNR=0 dB in Ex. 1.

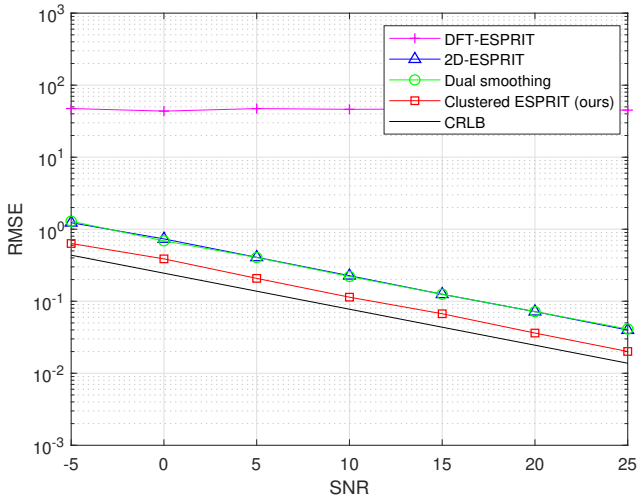

Fig. 13: RMSE of the angle estimates versus SNR with $Q = 2$ in Ex. 1.

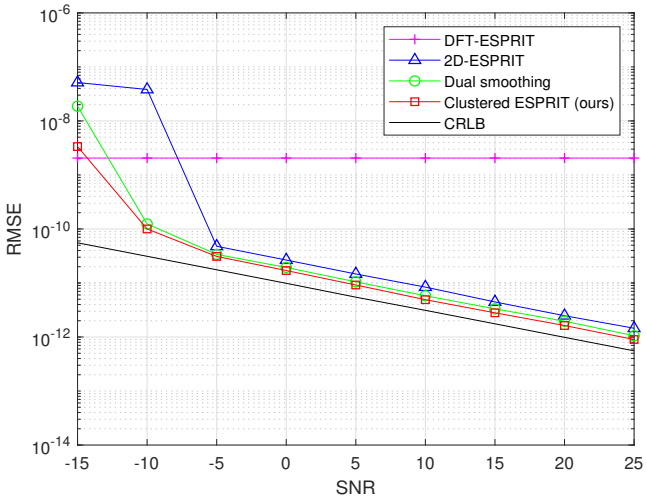

Fig. 15: RMSE of the time delay estimates versus SNR with $Q = 4$ in Ex. 2.

V. PRACTICAL EXPERIMENTS

This section validates the proposed algorithm by a practically implemented 24GHz ISM band FMCW radar device. As with the numerical simulations provided in the previous section, the considerations are general and invariant with respect to the specific scenarios considered. The photograph of this device is as shown in Fig. 18, which has one transmit antenna and two receive antennas. The transmitted FMCW sawtooth source with a short period around 0.571 msec is generated by the transceiver IC-BGT24 provided by the Infineon Technologies. This IC consists of a transmitter (Tx) chain and a receiver (Rx) chain. For the Tx chain, the frequency of FMCW is generated by a voltage-controlled oscillator (VCO). The frequency of VCO is controlled by the input voltage which is generated by the digital to analog (D/A) of microcontroller unit (MCU). The frequency of the generated FMCW source sweeps from 24.05 GHz to 24.25 GHz, *i.e.,* 200 MHz bandwidth. The FMCW source is amplified before it is sent out by the transmit antenna with the transmit radio frequency output power being 15 dBm. For the Rx chain, when the transmitted FMCW signal radiated by the transmitter hits the targets, the reflected waveform of the targets is received by the two receive antennas. The received waveform of the two channels are sent to the transceiver of IC-BGT24, amplified by a low-noise amplifiers with 10 dB gain, and then mixed with the output waveform of VCO. The mixer converts the 24 GHz signals directly down to zero-IF and offers differential in-phase and quadrature IF output signals. The beat signals are obtained by combining the in-phase and the quadrature-phase (I/Q) channel beat signals of the mixer output. The combined signals of the mixer output pass through a high pass filter with the cutoff frequency 16kHz, and a 20 dB amplifier, IC-ina827, provided by the Texas Instruments [21]–

1558-1748 (c) 2019 IEEE. Personal use is permitted, but republication/redistribution requires IEEE permission. See http://www.ieee.org/publications_standards/publications/rights/index.html for more information.

This article has been accepted for publication in a future issue of this journal, but has not been fully edited. Content may change prior to final publication. Citation information: DOI 10.1109/JSEN.2019.2949367, IEEE Sensors Journal

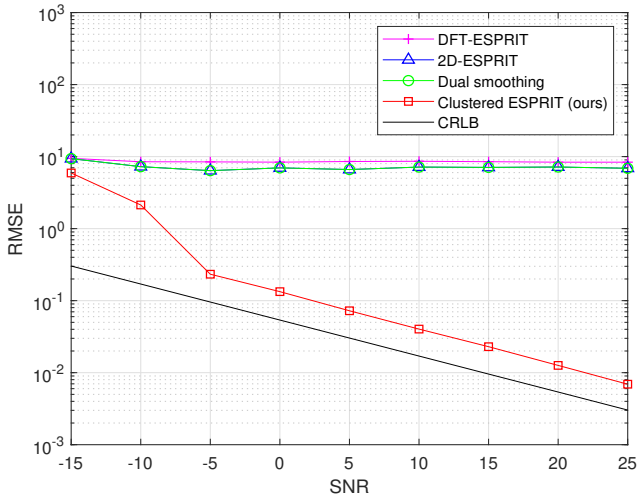

Fig. 16: RMSE of the angle estimates versus SNR with $Q = 4$ in Ex. 2.

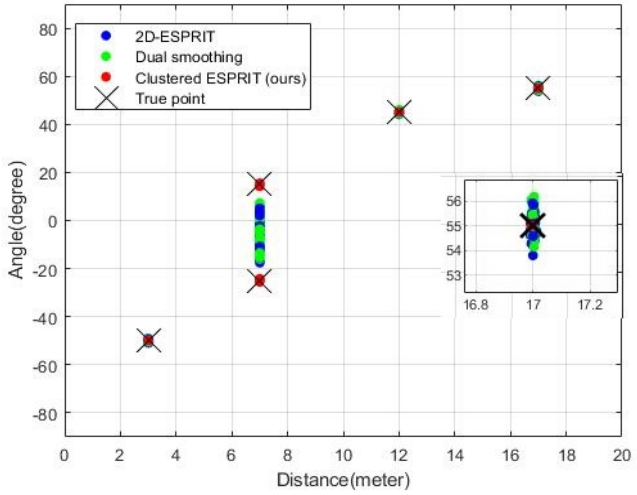

Fig. 17: The range-angle map of the targets with $Q = 4$ at SNR=0 dB in Ex. 2.

[24]. Afterward, one MCU-XMC 4400, provided by Infineon Technologies, is employed to perform the base band analog beat signals. This MCU has two ADCs with 12 bits resolution. The discrete I/Q signals in the two channels are obtained by conducting the ADCs with a sampling frequency of 448 KHz. The discrete I/Q signals of each channel are then combined and sent out via the built-in universal serial bus (USB) interference of XMC 4400 [25]–[29]. These data are then processed by the developed algorithm or baselines to estimate the ranges and angles of the targets.

To verify the performance of the proposed algorithm, two different experiments are carried out. Here only the results using 2D-ESPRIT, dual smoothing algorithm, and the proposed clustered ESPRIT are provided. DFT-ESPRIT is not considered, as it is not applicable in the scenarios when the number of the receive antennas is less than that of targets.

TABLE II: Comparisons of the RMSEs of the delay and angle estimates.

Algorithm	Chamber		Outdoor	
	Delay	Angle	Delay	Angle
2D-ESPRIT	3.7×10^{-10}	0.4568	8.1×10^{-11}	0.5312
Dual smoothing	3.6×10^{-10}	0.4568	1.8×10^{-10}	0.5312
Ours	1.1×10^{-10}	0.2678	1.2×10^{-10}	0.2675

To avoid the unknown echoes reflecting from the outer site, the first indoor experiment is performed in a chamber in the National Taiwan University of Science and Technology. The experiment setup is as shown in Fig. 19, where three 15cm equilateral aluminium triangular corners are regarded as targets and are located at $(R_1, \theta_1) = [2.3\,m, -35^o]$, $(R_2, \theta_2) = [5.4\,m, -23^o]$ and $(R_3, \theta_3) = [3.7\,m, 40^o]$. $N = 256$ samples are employed and the parameter $L = 85$ is used in (4). The experimental results based on the proposed algorithm and the other two baselines are as shown in Fig. 20, from which we can see that our algorithm can estimate the ranges and angles of the targets more precisely compared with the other two baselines, in which the estimates mostly center around the true locations of the targets.

The second experiment is conducted in an open field in the outdoor environment with three targets, which are located at bit farther locations, $(R_1, \theta_1) = [4.1\,m, -22^o]$, $(R_2, \theta_2) = [6.6\,m, 16^o]$ and $(R_3, \theta_3) = [9.8\,m, 50^o]$, as shown in Fig. 21. Again, we compare the proposed algorithm with the other two baselines, as shown in Fig. 22, from which we can see again that the new algorithm can yield more accurate range and angle estimates than the other two baselines. We can find that the estimates mostly center around the true location of the targets.

To further verify the estimation accuracy, we also compare the RMSE of the delay and angle estimates for both of the indoor (chamber) and outdoor environments based on the above algorithms, as shown in Table II. from which we can see that the results are in accord with the results in Figs. 20 and 22.

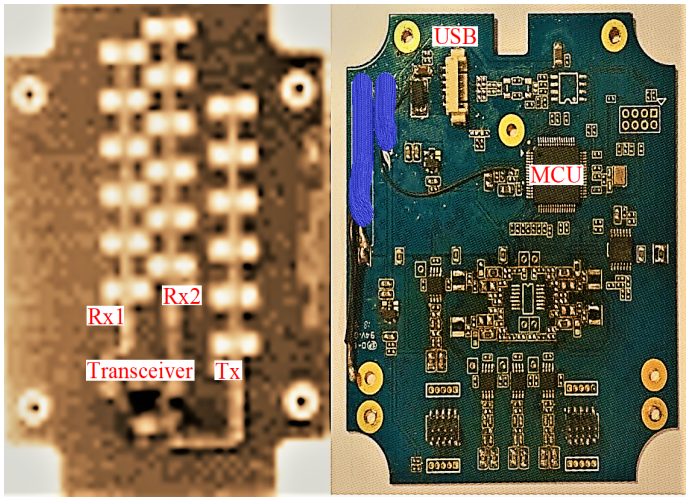

Fig. 18: Photograph of the employed FMCW radar device (pattern pending).

1558-1748 (c) 2019 IEEE. Personal use is permitted, but republication/redistribution requires IEEE permission. See http://www.ieee.org/publications_standards/publications/rights/index.html for more information.

This article has been accepted for publication in a future issue of this journal, but has not been fully edited. Content may change prior to final publication. Citation information: DOI 10.1109/JSEN.2019.2949367, IEEE Sensors Journal

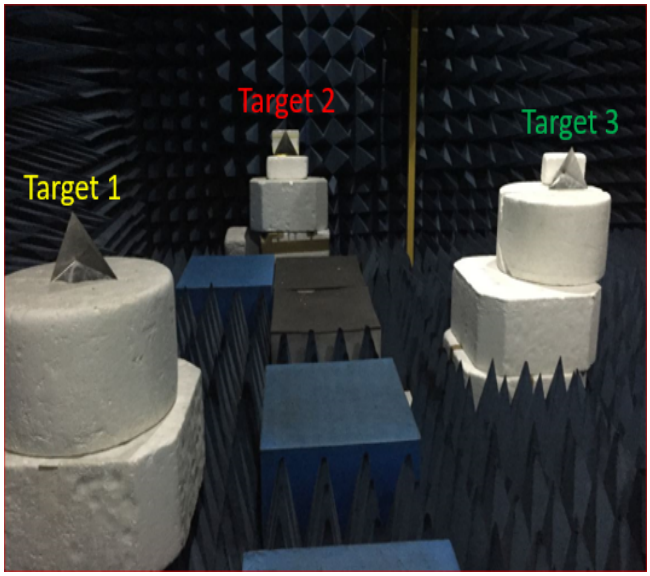

Fig. 19: The experiment scenario setup in the chamber.

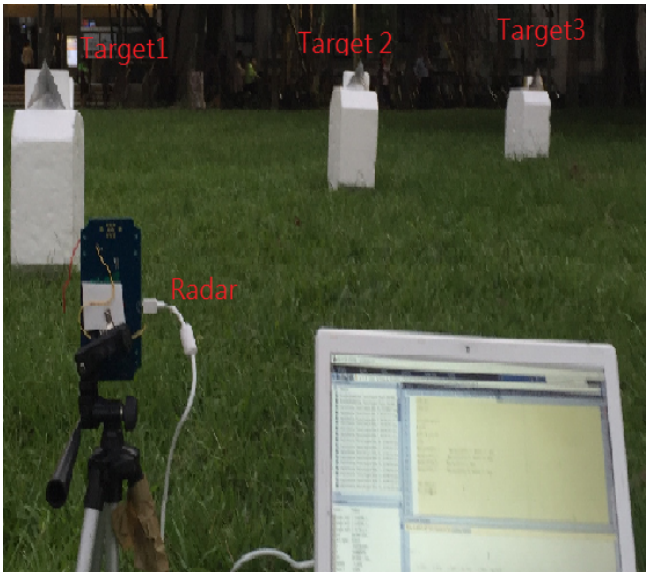

Fig. 21: The experiment scenario setup outdoor.

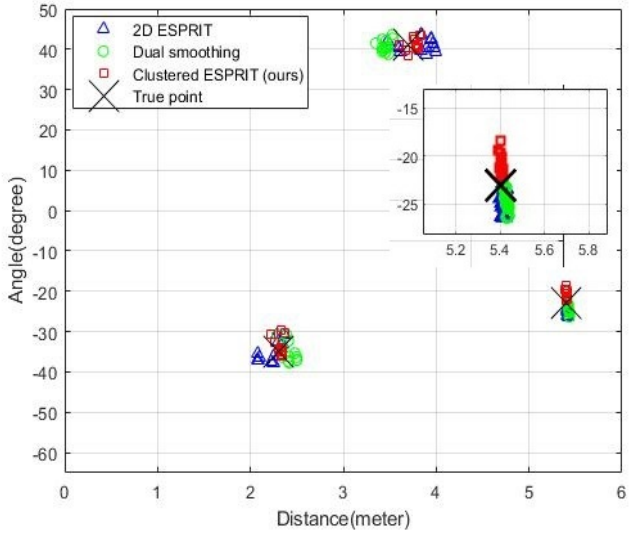

Fig. 20: Experimental results for three targets in the chamber, where targets are located at $(R_1, \theta_1) = [2.3\,m, -35^o]$, $(R_2, \theta_2) = [5.4\,m, -23^o]$, $(R_3, \theta_3) = [3.7\,m, 40^o]$.

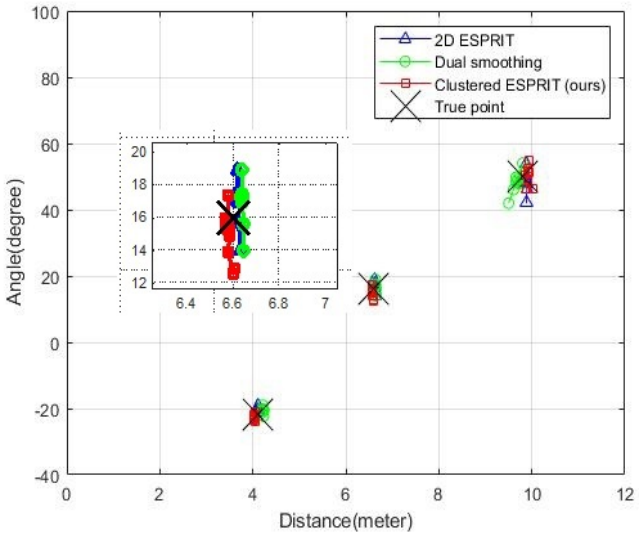

Fig. 22: Experimental results for three targets in the outdoor environment, where targets are located at $(R_1, \theta_1) = [4.1\,m, -22^o]$, $(R_2, \theta_2) = [6.6\,m, 16^o]$, $(R_3, \theta_3) = [9.8\,m, 50^o]$.

VI. CONCLUSION

This paper has developed an efficacious and efficient algorithm, clustered ESPRIT, for accurate angle and range estimation in the FMCW radar systems. The new algorithm uses ESPRIT for both range and angle estimation with the incorporation of a signal cluster process in between. Consequently, it is still applicable even if some targets have the same ranges or angles, and the estimated parameters are automatically paired together. Both numerical simulations and practical experiments are provided to validate the new algorithm.

ACKNOWLEDGMENT

We would like to express our gratitude to the associate editor and the reviewers for many thoughtful comments and suggestions which have enhanced the quality and readability of this paper. The help of Yung-An Chung and Tsai-Ling Yu in running some simulations is greatly appreciated. This work was supported by the Asuka company, which also provided the Radar chip set to experimentally validate the developed algorithm, and Ministry of Science and Technology, R.O.C. under contract MOST 107-2221-E-011-078-MY2.

REFERENCES

[1] S. Tokoro, "Automotive application systems of a millimeter-wave Radar," in *Proc. IEEE Intelligent Vehicles Symp.,* pp. 260-265, 1996.
[2] H. Rohling and C. Moller, "Radar waveform for Automotive Radar Systems and Applications," in *Proc. IEEE Radar Conf.,* pp. 871-876, May 2004.

1558-1748 (c) 2019 IEEE. Personal use is permitted, but republication/redistribution requires IEEE permission. See http://www.ieee.org/publications_standards/publications/rights/index.html for more information.

This article has been accepted for publication in a future issue of this journal, but has not been fully edited. Content may change prior to final publication. Citation information: DOI 10.1109/JSEN.2019.2949367, IEEE Sensors Journal

[3] W. Jones, "Building Safer Cars," *IEEE Specturm.,* vol. 39, no. 1, pp. 82-85, Jan. 2002.

[4] Y. Zhao and Y. Su, "Vehicle detection in complex urban scenes using Gaussian mixture model with FMCW radar," *IEEE Sensors Journal,* vol. 17, no. 18, pp. 5948-5953, Sep. 2017.

[5] V. Winkler, "Range Doppler detection for automotive FMCW radars," in *Proc. Eur. Microw. Conf.,* pp. 1445-1448, 2007.

[6] E. Hyun, W. Oh and J.-H. Lee, "Two-step moving target detection algorithm for automotive 77 GHz FMCW radar," in *Proc. IEEE Vehicular Tech. Conf.,* pp. 1-5, 2010.

[7] J. Choi, J. Park and D. Yeom, "High angular resolution estimation methods for vehicle FMCW radar," in *Proc. IEEE CIE International Conf. on Radar,* vol. 2, pp. 1868-1871, 2011.

[8] P. Wenig, M. Schoor, O. Gunther, B. Yang, and R. Weigel, "System design of a 77 GHz automotive radar sensor with super resolution DOA estimation," in *Proc. Int. Signals, Syst., Electron. Symp.,* pp. 537-540, 2007.

[9] R. O. Schmidt, "Multiple emitter location and signal parameter estimation," *in Proc. RADC Spectral Estimation Workshop,* Rome, pp. 243-258, NY. 1979.

[10] R. Roy and T. Kailath, "ESPRIT-Estimation of signal parameters via rotational invariance techniques," *IEEE Trans. Acoustics, Speech, and Signal Process,* vol. 37, no. 7, pp. 984-995, July 1989.

[11] F. Belfiori, W. van Rossum, and P. Hoogeboom, "Application of 2D MUSIC algorithm to range-azimuth FMCW radar data," in *Proc. Eur. Radar Conf.,* pp. 242-245, 2012.

[12] S. Kim, D. Oh and J. Lee, "Joint DFT-ESPRIT Estimation for TOA and DOA in Vehicle FMCW Radars," *IEEE Ant. and Wireless Propagation Letters,* vol. 14, pp. 1710-1713, Apr. 2015.

[13] D. Oh, Y. Ju and J. Lee, "Subspace-based auto-paired range and DOA estimation of dual-channel FMCW radar without joint diagonalisation, " *Electronics Letters,* vol. 50, No. 18, pp. 1320-1322, Aug. 2014.

[14] D. Oh, Y. Ju, H. Nam and J.-H. Lee, "Dual smoothing DOA estimation of two-channel FMCW radar," *IEEE Trans. Aerosp. Electron. Syst.,* vol. 52, no. 2, pp. 904-917, Apr. 2016.

[15] J. Gilbert and L. Gilbert, *Linear Algebra and Matrix Theory.* New Dehli, India: Academic, 2005.

[16] H. L. Van Trees, *Optimum Array Processing.* Wiley-Interscience, 2002.

[17] W.-H. Fang, Y.-C. Lee and Y.-T. Chen, "Importance sampling-based maximum likelihood estimation for multidimensional harmonic retrieval," *IEEE Signal Processing Letters,* vol. 23, no. 1, pp. 35-39, Jan. 2016.

[18] C.-H. Lin and W.-H. Fang, "Joint angle and delay estimation in frequency hopping systems,"*IEEE Trans. Aerospace and Electronic Systems,* vol. 49, no. 2, pp. 1042-1056, 2013.

[19] G. H. Golub and C. F. Van Loan, *Matrix Computations.* 3^{rd} ed. Johns Hopkins University Press, 1996.

[20] E. Aboutanios and B. Mulgrew, "Iterative frequency estimation by interpolation on Fourier coefficients," *IEEE Trans. Signal Process,* vol. 53, no. 4, pp. 1237-1242, Apr. 2005.

[21] M. Wang, T. Wang, Y. Sun, Y. Wu, Y. Zhou and X. Yang, "Automated FMCW Radar Experimental Platform," in *Proc. IEEE Advanced Information Management, Communicates, Electronic and Automation Control Conf.*, pp. 856-860, 2018.

[22] H.-N. Wang, Y.-W. Huang, and S.-J. Chung, "Spatial diversity 24-GHz FMCW radar with ground effect compensation for automotive applications," *IEEE Trans. Vehicular Technology,* vol. 66, no. 2, pp. 965-973, 2017.

[23] C. Deck, H.-J. Ng, R. Agethen, M. PourMousavi, H.-P. Forstner, M. Wojnowski, K.Pressel, R. Weigel, A. Hagelauer and D. Kissinger, "Industrial mmWave Radar Sensor in Embedded Wafer-Level BGA Packaging Technology," *IEEE Sensors Journal,* vol. 16, no. 17, pp. 6566-6578, Sep. 2017.

[24] E. Ozturk, D. Genschow, U. Yodprasit, B. Yilmaz, D. Kissinger, W. Debski and W. Winkler, "A 60-GHz SiGe BiCMOS Monostatic Transceiver for FMCW Radar Applications," *IEEE Trans. Microwave Theory and Techniques,* vol. 65, no. 12, pp. 5309-5323, 2017.

[25] D. Kurniawan, O. Heriana, T. Praludi and R. Sariningrum, "Data acquisition and signal processing on FMCW navigation radar system," in *Proc. Radar, Antenna, Microwave, Electronics, and Telecommunications,* pp. 45-52, Oct. 2017.

[26] A. Melzer, F. Starzer, H. Joger and M. Huemer, "Real-time mitigation of short-range leakage in automotive FMCW radar transceivers," *IEEE Trans. Circuits and Systems II: Express Briefs,* vol. 64, no. 7, pp. 847-851, July 2017.

[27] A. Anghel, G. Vasile, R. Cacoveanu, C. Ioana and S. Ciochina, "Short-range wideband FMCW radar for millimetric displacement measurements," *IEEE Trans. Geoscience and Remote Sensing,* vol. 52, no. 9, Sep. 2014.

[28] S. Aulia, A. B. Suksmono, A. Munir, "Stationary and moving targets detection on FMCW radar using GNU radio-based software defined radio," in *Proc. Intelligent Signal Processing and Communication Systems,* pp. 468-473, 2015.

[29] C. Will, P. Vaishnav, A. Chakraborty, A. Santra, "Human Target Detection, Tracking, And Classification Using 24 GHz FMCW Radar," to appear in IEEE Sensors Journal.

Wen-Hsien Fang Wen-Hsien Fang received the B.S. degree in Electrical Engineering from National Taiwan University in 1983, and his M.S.E. degree and Ph.D. degree from the University of Michigan, Ann Arbor, in 1988 and 1991, respectively, in electrical engineering and computer science. In fall 1991, he joined the faculty of National Taiwan University of Science and Technology, where he currently holds a position as a professor in the Department of Electronic and Computer Engineering. His research interests include statistical signal processing, computer vision, and machine learning.

Li-Der Fang Li-Der Fang received the B.S. degree from Chung Yuan Christian University in 1990, and his M.S.E. degree from Chung Cheng Institute of Technology in 1998, both in electrical engineering. He spent most of his career in the Army, where he was responsible for radar and communication system development. He is currently pursuing the Ph.D. degree in the Department of Electronic and Computer Engineering of National Taiwan University of Science and Technology. His research interests is to apply signal processing to radar applications.

1558-1748 (c) 2019 IEEE. Personal use is permitted, but republication/redistribution requires IEEE permission. See http://www.ieee.org/publications_standards/publications/rights/index.html for more information.